University of Mohaghegh Ardabili

Research Paper

Enhanced DC Microgrid Protection: A 2D Current Modeling and Deep Learning Approach

Behrooz Taheri [1] , *Seyed Amir Hosseini* [2, *] , and *Mostafa Sedighizadeh* [3]

[1]*Department of Electrical Engineering, Qazvin Branch, Islamic Azad University, Qazvin, Iran.*
[2]*Electrical and Computer Engineering Group, Golpayegan College of Engineering, Isfahan University of Technology, Golpayegan, Iran.*
[3]*Faculty of Electrical Engineering, Shahid Beheshti University, Evin, Tehran, Iran.*

Abstract— *This paper introduces a novel protection method for identifying and locating faults in DC microgrids, which is aimed at overcoming the challenges faced by modern power systems. A two dimensional current modeling technique is utilized to detect faults, in which even minimal changes in the sampled data result in rapid detection due to the model's sensitivity. Additionally, the method differentiates between transient and permanent faults and is robust against noise in sampled signals. Furthermore, a deep learning model based on long short term memory layers, optimized using the whale optimization algorithm, is applied for fault location. The deep learning model's layers are fully aligned with the data, and the optimization process enhances the model's accuracy. The proposed scheme operates without relying on extensive communication links, making it practical for real world applications. Comparative evaluations demonstrate that the system outperforms existing methods in terms of accuracy, speed, and reliability, confirming its effectiveness in DC microgrid protection. The deployment of the proposed method effectively identifies and pinpoints faults at various locations within the microgrid in as little as 1 millisecond and within PV and EV components in up to 11 milliseconds. This capability has been validated across a range of fault types and impedances. Additionally, the method has demonstrated reliable performance despite noisy conditions, maintaining accuracy with a signal to noise ratio of 40 dB.*

Keywords—DC microgrid, microgrid protection, two dimensional modeling, deep learning model.

1. Introduction

The DC nature of many renewable distributed generations (DGs), along with the increase in DC loads, makes it necessary to develop DC microgrids (DCMG) with the ability to directly connect these sources and loads [1]. Additionally, DCMGs exhibit higher efficiency, lower losses, and greater power transmission capacity than their AC counterparts [2, 3]. In contrast to AC microgrids, DCMGs do not require control of reactive power, frequency, or synchronization [4]. Despite these advantages, the development of DCMGs still faces various challenges, with the most significant challenge being protection issues in these microgrids [1].

The protection process of these microgrids is complicated by factors such as the nature of the fault current, the types of possible faults, the fault's location, and the transient states in these networks. For instance, the rapid discharging of capacitors in the DC link of converters during a fault can lead to a fault current amplitude that reaches 100 times the rated current in a very short time [5, 6]. This heightened current amplitude poses a significant risk of causing severe damage to the power electronic devices

within these networks [7]. Consequently, there is a pressing need for the development of fast fault detection (FD) and location (FL) methods in these microgrids [2]. The developed FD method should be capable of distinguishing between permanent faults and transient states in the microgrid [8]. Moreover, within these microgrids, the switching of power electronic devices induces a transient state and noise, which may erroneously be identified as faults by FD algorithms [9]. Furthermore, the fault type in DCMGs differs significantly from that in AC microgrids. Specifically, pole to pole (PP) and pole to ground (PG) faults are potential fault types within DCMGs [10]. These faults occur in DC buses, DC lines, and elements connected to lines and DC buses, including converters, various types of loads, and renewable DGs [10]. Therefore, it is essential to develop a method for locating faults in these networks, taking into account the various potential locations where faults can occur.

So far, numerous studies have been conducted in the field of FD and FL in DCMGs. Consequently, various schemes have been proposed in studies for FD in DCMGs, including overcurrent protection ([11, 12]), current variations over time ([13, 14]), distance protection ([15, 16]), traveling waves ([17, 18]), intelligent methods ([19, 20]), and signal processing ([9, 21]). Differential protection methods using current [22], frequency based current [23], DC bus power gradient [24], Shannon entropy [25], and Synchro Squeezing Transform [26] have also been proposed for FD in DCMGs. In addition to the mentioned methods, there are also techniques for detecting faults in the components of DCMGs. For example, reference [27] employs the characteristics obtained from the two dimensional (2D) curve of photovoltaic (PV) current voltage to train various intelligent methods for FD in PV arrays. Similarly, reference [28] has presented a FD method for PV

arrays based on the determinism parameter of DC voltage signals obtained from recurrence plots. A recurrence plot is a nonlinear analysis method for time series, enabling the creation of a 2D plot illustrating signatures of system parameter signals.

While FD is crucial for safeguarding power converters in DCMGs, accurate FL with high speed is equally important to prevent equipment damage and minimize downtime through swift repairs [29]. However, achieving this presents several challenges. Fault response characteristics depend heavily on factors like fault resistance, type, and location within the network [30]. Additionally, DCMGs are inherently susceptible to faults at various locations, further complicating the issue. The dynamic nature of these grids, with DGs, electric vehicles (EVs), and energy storage systems, introduces uncertainties in network topology [9]. Consequently, a robust FL method is necessary to effectively pinpoint FLs despite these variations. Therefore, various FL schemes have been proposed for both online and offline implementations. In offline schemes, FL occurs after its detection. In these schemes, a probe power unit is employed to inject current into the FL [29, 31]. However, this approach raises the cost and time required for implementing the method [32]. Conversely, FL in online schemes is performed simultaneously with the FD process. Yet, the absence of frequency and phasor information in DCMGs, unlike AC networks, renders methods based on impedance calculation unusable for online FL [30]. This necessitates alternative approaches based on measured voltage and current data [33]. Accordingly, traveling wave based methods have been proposed for FL in DCMGs [34]. However, the short cable lengths in these grids make it difficult to distinguish reflected waves, limiting their effectiveness [30]. Additionally, differential protection methods, while suggested in some studies [35, 36], require communication links which may not always be available or reliable.

The limitations of traditional FD and FL methods in DCMGs, particularly their dependence on specific network configurations, have spurred the exploration of artificial intelligence (AI) algorithms [19, 36, 37]. Several studies, including references [19, 36], propose using artificial neural networks (ANNs) for both FD and FL. However, these specific ANN based methods are limited to DC bus faults within a fixed microgrid topology. In reference [37], the authors introduce a novel approach combining machine learning and deep learning for FD and FL. They begin by employing a regression tree model to identify faults within the DCMG. Subsequently, a long short term memory (LSTM) deep learning model is used to pinpoint the precise location of the fault. The most important challenge of this method is its poor performance when the signal becomes noisy.

In general, the challenges of the presented methods for FD and FL in DCMGs can be categorized into the following points:

1. The need for high performance response times due to the sharp increase in fault current amplitude in a short period of time [2, 5, 6].

2. Various locations prone to faults in the DCMG and the equipment connected to it, along with the uncertainty in the microgrid topology due to the presence of DGs, energy storage systems, and EVs.

3. Limiting the use of communication links, especially in differential protection schemes, due to the operational uncertainty of these links [38].

4. The nonlinear nature of converters poses a challenge for impedance calculation in distance protection based methods [16].

5. The absence of accurate FD and FL under noisy signal conditions [39] and the lack of correct differentiation between transient states and permanent network faults [8].

6. Neglecting converter control strategies in DCMG protection. These strategies can introduce transient events that can adversely affect protection schemes and their effectiveness [40].

7. The short length of microgrid lines poses a limitation for using traveling wave schemes [41].

As demonstrated, it is clear that the protection of DCMGs

remains a fundamental challenge and a primary obstacle to the expansion of these networks. To address this issue, this paper introduces a comprehensive FD and FL scheme that utilizes only one intelligent electronic device (IED) for DCMG protection. The adoption of a single IED significantly reduces microgrid protection costs and eliminates the challenges associated with uncertainties in communication links. The proposed FD approach in DCMGs is rooted in 2D current modeling. Moreover, to ensure precise FL and mitigate the increase in outage incidents, a deep learning model, namely the LSTM, has been employed. To achieve the most optimal performance of the LSTM deep learning model, its adjustment parameters are optimized by the whale optimization algorithm (WOA). To assess the effectiveness of the proposed method, simulations were carried out in a DCMG using Simulink in MATLAB, including components like photovoltaic (PV) systems, EVs, and hybrid energy storage systems (HESS) consisting of flywheels and batteries. It is noteworthy that the controllers of DCMGs, particularly those of HESS, have a significant impact on the protection algorithms [42]. Consequently, the microgrid hierarchical control system is fully implemented based on the control system proposed in [43]. The simulation results demonstrate the method's efficiency and ability to quickly identify various types of faults in the DCMG. Moreover, the LSTM model employed for FL exhibits high accuracy. This paper also conducts a comprehensive comparison between different established techniques for identifying and locating faults in DC networks and the proposed approach. The results demonstrate the favorable performance of the proposed method. In summary, the innovations in this paper can be outlined as follows:

1. Introduction of a novel FD method based on 2D current modeling for rapid FD in DCMGs.

2. Integration of WOA and LSTM deep learning models to enhance the protection algorithm and achieve reliable FL in DCMGs.

3. Utilization of a single IED in the proposed method.

4. Consideration of EV, PV, and HESS.

5. Complete implementation of the control system and analysis of the impact of transients generated by it on the performance of the proposed protection method.

This paper is organized as follows: The second section introduces the FD method based on 2D current modeling and the proposed WOA-LSTM model for FL. The third section discusses simulation results for the DCMG containing EV, PV, and HESS. In the fourth section, the proposed method is compared with techniques found in different references.

2. PROBLEM FORMULATION

2.1. Sample microgrid

This paper utilizes a DCMG comprising EV, PV, and HESS systems, as outlined in [43], to assess the effectiveness of the proposed protection algorithm. Integrating HESS can introduce transients into the microgrid, potentially resulting in the failure and maloperation of the protection system. Furthermore, the presence of EV and PV in the microgrid, known for their high uncertainty in power consumption and production, can induce errors in conventional network protections such as overcurrent relays. Fig. 1 illustrates the sample microgrid utilized for evaluation [44]. The parameters of this network are provided in the appendix [43]. The placement of the IED responsible for sampling the required signals on the network is shown in Fig. 1. According to the figure, this IED is installed at the DC bus.

A microgrid with the outlined components necessitates an appropriate control system to ensure accurate performance. Therefore, the hierarchical control system described in [43] has been completely integrated into this study. It is worth noting that the central controller system and communication links, as illustrated in the figure, correspond to the control system outlined in [43]. The sample microgrid is simulated using Simulink in

MATLAB. Additionally, both the proposed protection algorithm and the LSTM model have been implemented within this software environment.
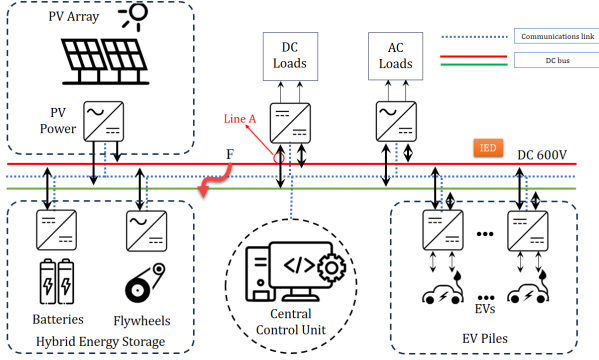

Fig. 1. The sample DCMG.

2.2. Detecting faults in DCMGs

This paper focuses on detecting faults within DCMGs through 2D current modeling. In essence, 2D modeling entails converting time series data into the geometric structure of an object within a defined space. [45]. The features extracted from 2D modeling contain more information than the raw time series signal [45]. Therefore, in this paper, the features obtained from 2D modeling within a signal window are utilized for fault detection.

To construct a 2D model, the current signal must be sampled by an IED. It's important to note that in the proposed method, only the point where the microgrid connects to the main grid is sampled, eliminating the need for multiple IEDs. Then, the current signal undergoes Fast Fourier Transform (FFT) using Eq. (1) to extract the fundamental frequency.

$$X_K = \sum_{n=0}^{N-1} I_n \times e^{-i2\pi K n/N} \quad , K = 0, ..., N-1 \tag{1}$$

where X_K represents the output obtained from the FFT, I_n is the n-th current sample input to the FFT, and N is the total number of data.

Accordingly, after applying the FFT to the current signal, the output yields complex numbers representing the amplitude and angle of the signal. Next, the real and imaginary parts are extracted based on Eqs. (2) and (3), forming the X and Y axes of the coordinate system.

$$X_n = \text{Real}(X_K) \tag{2}$$

$$Y_n = \text{Imag}(X_K) \tag{3}$$

Fig. 2 depicts the changes in X and Y values on the coordinate system under different conditions (normal conditions/fault occurrences) of the microgrid. As illustrated, the distance between the generated points and the coordinate center exhibits a notable difference under various conditions. This characteristic serves as a means to distinguish between normal conditions, transients induced by the control system, and faults in the microgrid. Based on this observation, the value of the summation of distances from each point relative to the coordinate center (SDTC) can be calculated as a significant feature during a signal window using Eq. (4) [45].

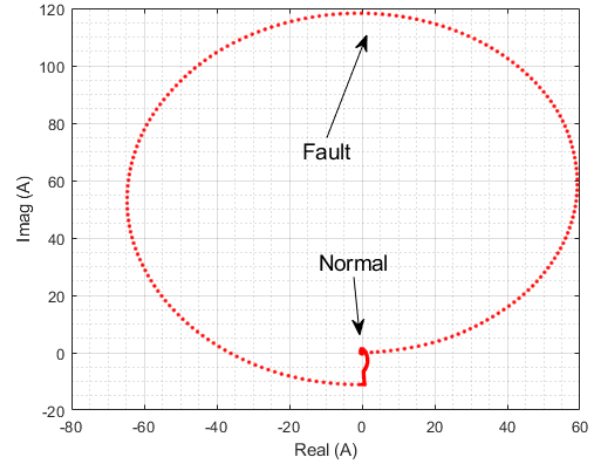$$SDTC = \sum_{n=1}^{N} \sqrt{X_n^2 + Y_n^2} \tag{4}$$

Fig. 2. Changes of X and Y values on the coordinate system in different microgrid conditions.

Indeed, the determination of a suitable sampling rate and window length is crucial for implementing the proposed protection method. The selection of an appropriate sampling rate can directly affect the accuracy and speed of protection techniques. Additionally, as emphasized in [44], the transients generated by the control system can directly influence the behavior of the protection system. Therefore, protection algorithms should be designed with these transients in mind, or alternatively, the protection system should be designed in a manner that minimizes the impact of transients created by the control system.

In the initial phase, it is necessary to define an appropriate sampling rate to determine these two parameters. To accomplish this, Fig. 3 illustrates the 2D modeling and SDTC at different time points using sampling rates of 10 kHz, 2 kHz, and 1 kHz. It is worth mentioning that the utilized sampling rates are common rates for protection algorithms. The figure clearly demonstrates that when using a sampling rate of 10 kHz, due to the high number of sampled points, the transients created by the control system result in a greater impact compared to the 1 kHz and 2 kHz sampling rates. However, during the fault, the calculated SDTC value significantly increases across all three sampling rates. Notably, when utilizing a sampling rate of 1 kHz, the FD time amounts to 18 ms, whereas the same detection time decreases to 1.8 ms when using a sampling rate of 10 kHz. This difference is crucial in FD time, particularly in DC systems. Consequently, a 10 kHz sampling rate is selected for use in this paper. Moreover, to mitigate the impact of transients generated by the control system, defining a threshold value is crucial for fault detection. Various types of faults and transient states are initially simulated within the network. Subsequently, the peak value is calculated for each state, and the threshold value is derived based on the peak values obtained from the different fault types and transient states. This threshold value has been determined as 18.

After determining an appropriate sampling rate, it is necessary to determine the size of the signal window. In AC systems, the size of the signal window is obtained using Eq. (5).

$$\text{Windowslength} = \frac{F_s}{F} \tag{5}$$

where F_s is the sampling frequency (10 kHz) and F is the nominal frequency of the system. Due to the lack of frequency in DCMGs, we use the frequency of the AC side, i.e., 50 Hz.
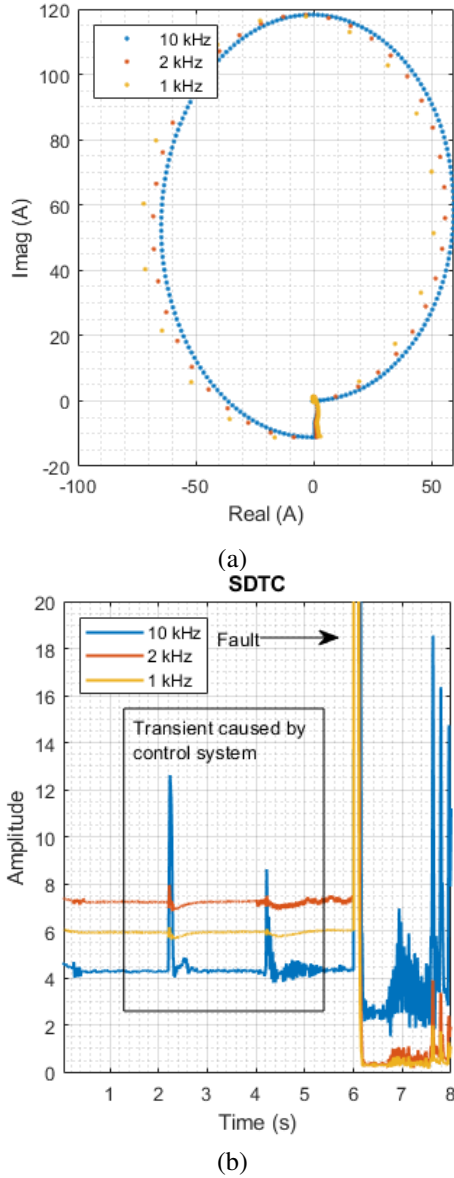
(a)

(b)

Fig. 3. Variation of X and Y values on the coordinate system and SDTC obtained over time at different sampling rates: a) 2D model, b) SDTC per time.

In conclusion, the fault is detected if the calculated SDTC value exceeds the threshold value (T). Otherwise, the generated transients are related to the control system or common network events. Accordingly, the FD condition can be formulated according to Eq. (6).

$$\text{IF}(\text{SDTC} > \text{T}) \rightarrow \text{Faultdetect} \tag{6}$$

2.3. Locating faults in DCMGs

Addressing FL in the DCMG is also another challenge that should be considered when using a single IED. Therefore, to tackle this challenge, a comprehensive protection algorithm utilizing the LSTM has been proposed in this section to locate the faults in the microgrid. The LSTM model, as a deep learning model, has been employed to address this issue. It is presented as a highly effective and scalable model. Moreover, the LSTM model overcomes the issues encountered in simple recurrent networks and has been utilized to solve numerous challenging problems [46, 47].

LSTM employs a memory cell capable of retaining its state over time, which is its distinguishing feature [48]. This model exhibits superior performance compared to existing neural networks in complex problems [49–52]. The structure of the LSTM model is depicted in Fig. 4 [53]. Furthermore, the relationships governing this model are illustrated by Eqs. (7)-(12) [54].

$$f_t = \sigma\left(W_f.\left[h_{t-1}, x_t\right] + b_f\right) \tag{7}$$

$$i_t = \sigma\left(W_i.\left[h_{t-1}, x_t\right] + b_i\right) \tag{8}$$

$$o_t = \sigma\left(W_o.\left[h_{t-1}, x_t\right] + b_o\right) \tag{9}$$

$$\tilde{C}_t = \tanh\left(W_C.\left[h_{t-1}, x_t\right] + b_c\right) \tag{10}$$

$$C_t = f_1 \odot C_{t-1} + i_t \odot \tilde{C}_t \tag{11}$$
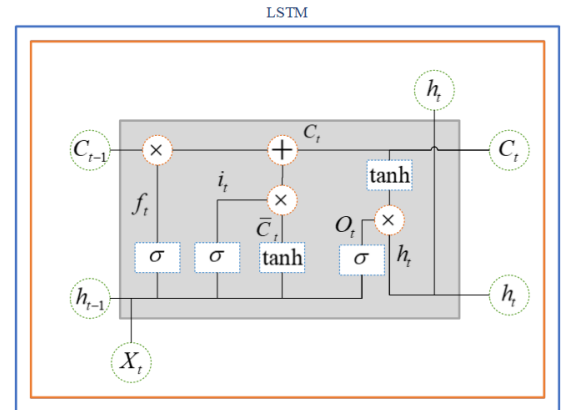
$$h_t = o_t * \tanh\left(C_t\right) \tag{12}$$

Fig. 4. LSTM model.

The parameters appearing in Eqs. (7)-(12) are specified in Table 1.

According to the research conducted in [55], it can be asserted that defining the number of neurons and repetitions of the model in the hidden layer of LSTM is a very challenging task. Numerous studies resort to manual configuration of these settings, but the number of hidden layers and the number of iterations can directly affect the performance of the model. For this reason, various studies, including [55–57] have used the particle swarm optimization (PSO) algorithm to optimize LSTM parameters. Although these studies have suggested a suitable improvement in the performance of the LSTM model, it is essential to state that the PSO algorithm demands a significant number of iterations to reach precise solutions, and additionally, this algorithm has a relatively low convergence accuracy [58]. Therefore, an appropriate optimization algorithm is needed to effectively optimize LSTM parameters.

The WOA was first introduced in [59]. In contrast to other algorithms, WOA stands out for its simplicity, with few parameters and optimal performance. This algorithm demonstrates superior global and local search capabilities. The optimization algorithm operates based on the simulation of whale behavior in their natural environment [60]. The WOA algorithm assumes that the currently

Table 1. Parameters of the LSTM Model.

f_t, i_t, o_t	Forget, input and output gates respectively.
σ	The sigmoid function.
x_t	Value of the current input.
h_{t-1}	Value of the previous output.
C_t	Cell state.
$\tilde{C}_t$	Value for calculating the current cell state.
C_{t-1}	Updated from previous cell state.
h_t	Output of current LSTM.

optimal selected solution is the target bait or close to the optimal point. Once the best search agent is identified, other search agents will try to update their positions toward the best search agent. This behavior can be mathematically expressed by Eqs. (13) and (14) [59].

$$\vec{D} = \left| \vec{C}.\vec{X} * (t) - \vec{X}(t) \right| \tag{13}$$

$$\vec{X}(t + 1) = \vec{X} * (t) - \vec{A}.\vec{D} \tag{14}$$

In the above equations, t represents the current iteration, $\vec{A}$ and $\vec{C}$ are coefficient vectors, $\vec{X}*$ is the position vector of the best solution obtained so far, and $\vec{X}$ is the position vector. It should be noted that $\vec{X}*$ should be updated in each iteration if there is a better solution. Vectors $\vec{A}$ and $\vec{C}$ are also calculated based on Eqs. (15) and (16) [59].

$$\vec{A} = 2\vec{a}.\vec{r} - \vec{a} \tag{15}$$

$$\vec{C} = 2.\vec{r} \tag{16}$$

During the exploration and productivity phases, the value of $\vec{a}$ gradually decreases from 2 to 0 over the iteration period, while $\vec{r}$ is a randomly generated vector ranging from 0 to 1 [59].

The position (X, Y) of a search agent can be updated based on the position of the current best value $(X*, Y*)$. Adjusting the values of the vectors $\vec{A}$ and $\vec{C}$ enables obtaining various locations around the best operator relative to the current position.

The WOA algorithm begins the optimization process by generating an initial set of random solutions. In each iteration, the search agents adjust their positions based on either a selected agent at random or the optimal solution identified up to that point. A random search agent is chosen when $\left| \vec{A} \right| > 1$, whereas the best solution is selected to update the position of search agents when $\left| \vec{A} \right| > 1$. Depending on the value of p, the WOA can transition between a helical and a circular motion. Ultimately, the WOA algorithm halts upon satisfying a predefined stopping criterion [59].

As noted earlier, the suggested method employs the WOA algorithm to refine the parameters of the LSTM model. The objective function, defined using the mean absolute percentage error (MAPE), is represented by Eq. (17) [60].

$$\text{Costfunction} = MAPE(h, y) = \frac{1}{n} \sum_{i=1}^{n} \left| \frac{h(i) - y(i)}{y(i)} \right| \tag{17}$$

where $h(i)$ represents the i-th estimated value and $y(i)$ represents the i-th actual value. The accuracy of the estimation value is inversely proportional to the loss value, indicating that a more accurate estimation results in a lower loss value.

Fig. 5 illustrates the LSTM model training and testing algorithm. Initially, the fault voltage and current are sampled for training (both voltage and current fundamental phasors [61]).
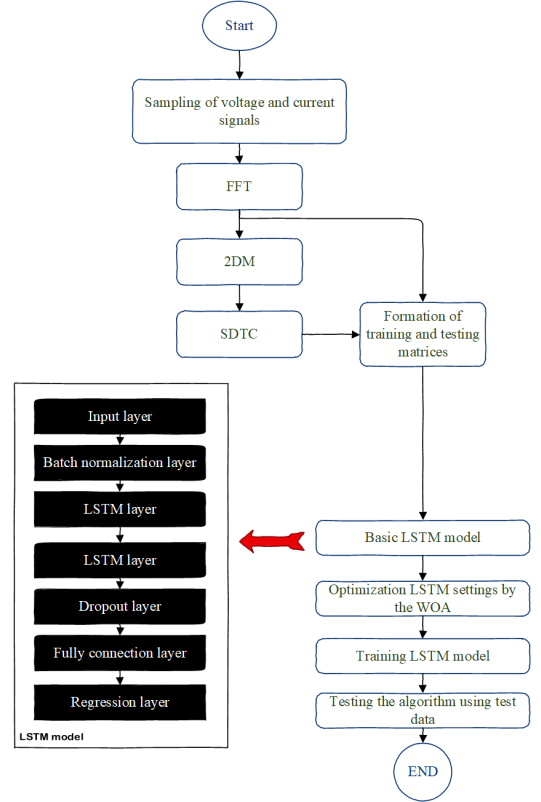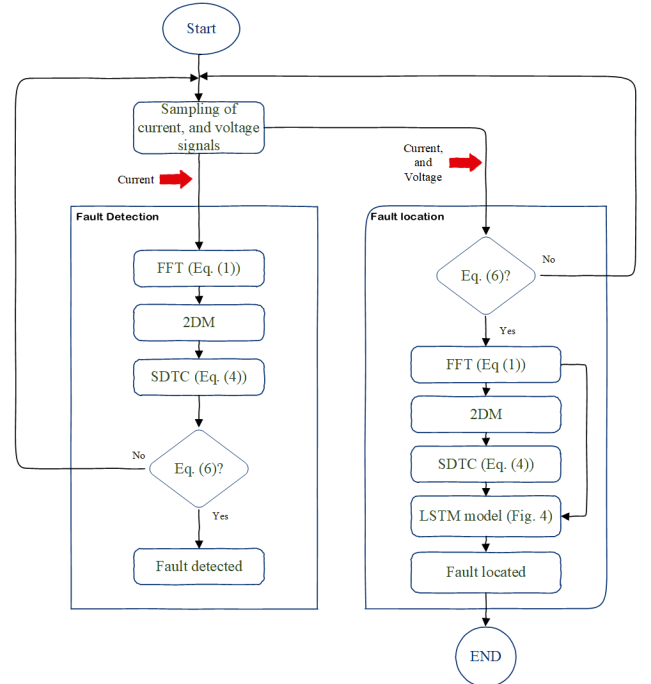

Fig. 5. LSTM model training and testing algorithm.

Fig. 6. Proposed protection algorithm.

2.4. Proposed protection algorithm

In the preceding sections, the FD and FL methods were discussed separately. In this section, we will present and examine the complete algorithm of the protection system, as demonstrated in Fig. 6. As evident from this algorithm, the FD process begins
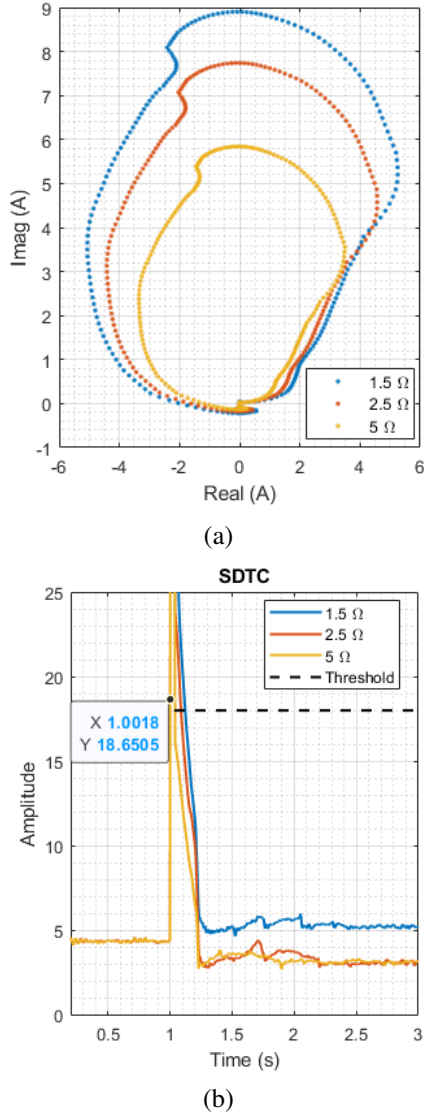
(a)

(b)

Fig. 7. Analysis of the proposed approach during PG fault scenarios, a) 2D model, b) SDTC over time.

(a)

(b)

Fig. 8. Analysis of the proposed approach during PP fault scenarios, a) 2D model, b) SDTC over time.

with the sampling of the microgrid current signal. Subsequently, the FFT is applied to the sampled current signal, and based on the FFT results, a 2D modeling process is executed. Next, the value of the SDTC is calculated. Finally, if the calculated SDTC value exceeds the predetermined threshold, the algorithm detects the fault. Following the FD phase, the algorithm progresses to the FL step. In this phase, the sampled current and voltage signals, along with the calculated SDTC value, are inputted into the pretrained LSTM model (as shown in Fig. 5) to ascertain the precise location of the fault.

3. SIMULATION RESULTS

3.1. Simulation results for implementing the proposed FD method

A) Investigating FD capability within the microgrid

The first stage in evaluating the proposed method involves testing its ability to identify different types of faults in the DCMG. Initially, a fault is introduced on the DC bus at t=1 second. For a thorough assessment, both PG and PP fault types are examined. Additionally, recognizing that fault impedance can notably influence detection algorithms, various fault impedances,
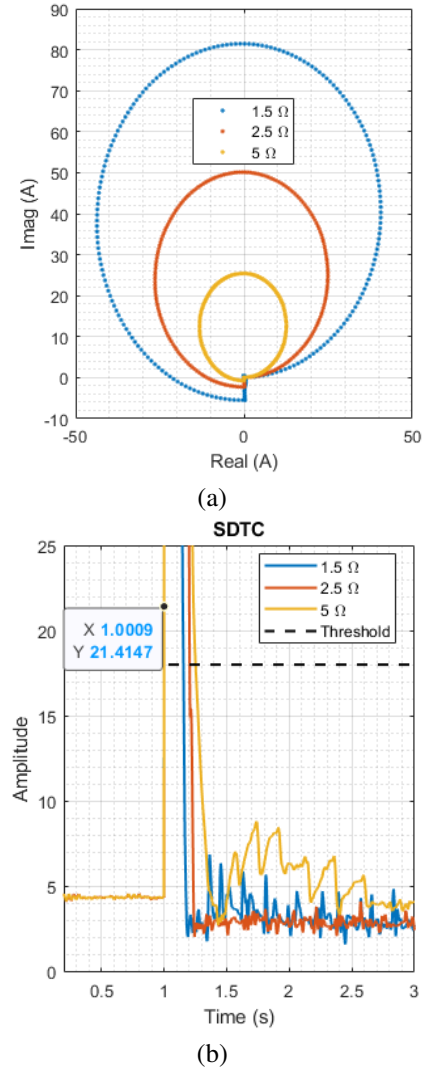
1.5Ω, 2.5Ω, and 5Ω, are also taken into account. Fig. 7 illustrates the performance of the proposed fault detection method under PG fault across different fault impedances. In Fig. 7-a, the extent of 2D modeling of the current is depicted. It's evident from this figure that the distance of the samples from the origin of the coordinates increases at the time of the fault occurrence. Consequently, as shown in Fig. 7-b, at t=1 second (the time of the fault occurrence), the calculated SDTC value surpasses its threshold value. Furthermore, Fig. 8 illustrates the operation of the proposed technique under PP faults with varying fault impedances. According to the simulation results depicted in these figures, the calculated SDTC value exceeds the predetermined threshold value during a fault occurrence, and the algorithm accurately detects both PG and PP faults across different fault impedances in approximately 1 ms.

B) Investigating FD capability within the EV chargers

To evaluate the capability of the proposed approach in detecting various fault types occurring within EV chargers, PG and PP faults with different fault impedances occur at t=1 second. These faults are located after the DC/DC converter and within the EV charger area. Fig. 9 illustrates the performance of the proposed approach when a PG fault occurs in the EV charger, while the performance of this approach when a PP fault occurs is depicted in Fig. 10. As evident from both figures, the calculated SDTC value at the time
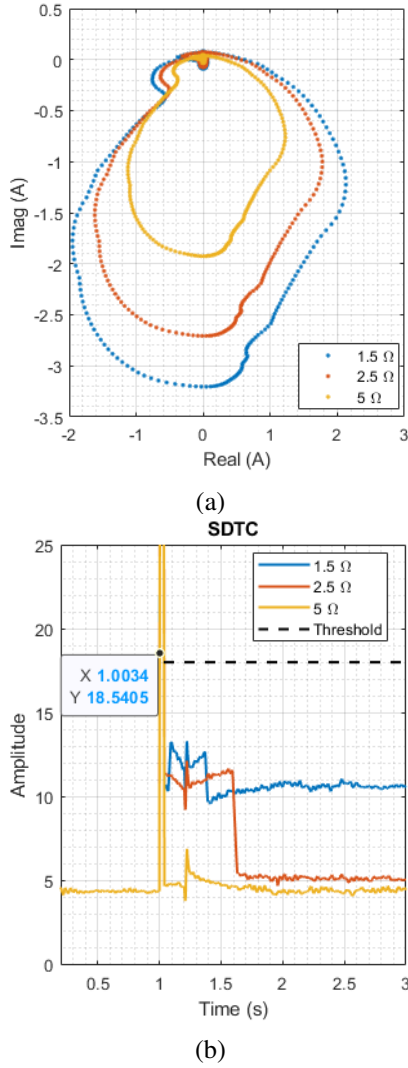
(a)

(b)

Fig. 9. Analysis of the proposed approach during PG fault scenarios within EV chargers, a) 2D model, b) SDTC over time.

(a)

(b)

Fig. 10. Analysis of the proposed approach during PP fault scenarios within EV chargers, a) 2D model, b) SDTC over time.

of the fault surpasses the threshold value, enabling the detection of the PG and PP faults in 3 ms and 11 ms, respectively. It should be noted that during the PP fault, EVs are considered to be in their vehicle to grid (V2G) operating mode, resulting in their unintentional contribution to the fault current. Consequently, an increase in FD time can be observed when the PP fault occurs in this part of the microgrid.

C) Investigating FD capability within the PV sources

This section evaluates how effectively the proposed method detects different faults in the converters of PV sources integrated into the microgrid. To test this, PP and PG faults are introduced in the DC-DC converter associated with PV systems at t=1 second. Figs. 11 and 12 present the performance results of the method for PG and PP faults, respectively. These figures show that the proposed approach successfully identifies PG faults within 1 ms and PP faults within 10 ms.

Table 2 presents a summary of the results obtained from the FD investigations. The data in this table clearly indicates that the proposed method exhibits rapid performance during various fault conditions. Additionally, the algorithm accurately identifies transient situations in the microgrid and does not operate under these conditions.
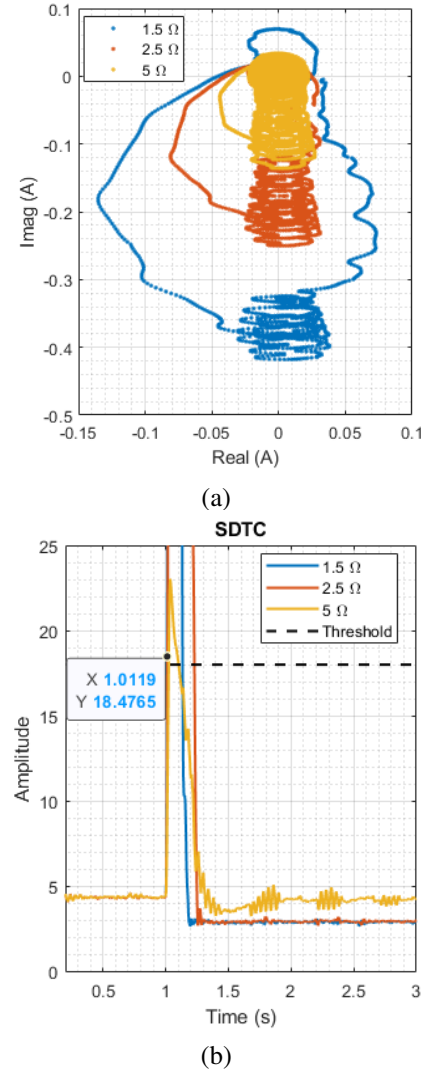
D) Investigating the ability to differentiate between fault conditions and transient states in the microgrid

In this section, we investigate the impact of transients occurring in the microgrid on the operation of the proposed method. Based on this, the power produced by PV is halved at t=2 seconds. Concurrently, the flywheel storage device begins injecting power into the microgrid to compensate for the power reduction. Later, at t=4 seconds, the power drawn by available loads abruptly doubles. This surge in consumption prompts the batteries to contribute by injecting power into the microgrid to compensate for the shortfall. To further enhance the complexity and assess the algorithm's performance, the power consumption of EV chargers is decreased due to a reduction in the number of vehicles being charged (at t=6 seconds). Consequently, this results in a decrease in the power contribution by the flywheel to the network. All these scenarios give rise to the occurrence of three significant transient states in the network. It should be noted that during these evaluations, the microgrid is in an islanded mode. The performance of the proposed method under these three transients is shown in Fig. 13. Notably, the computed SDTC value remains below the threshold throughout all the examined transients, and the algorithm shows no operation for these conditions.
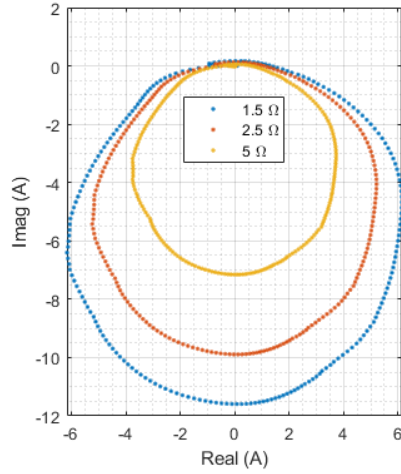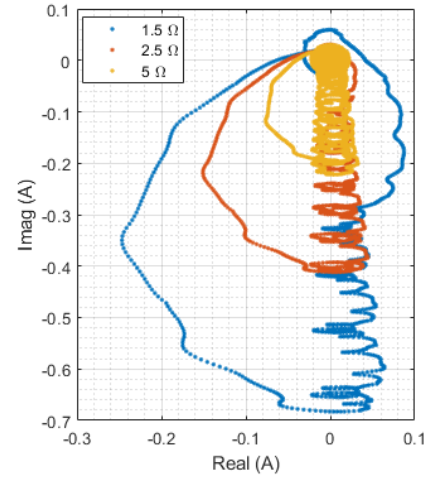
(a)
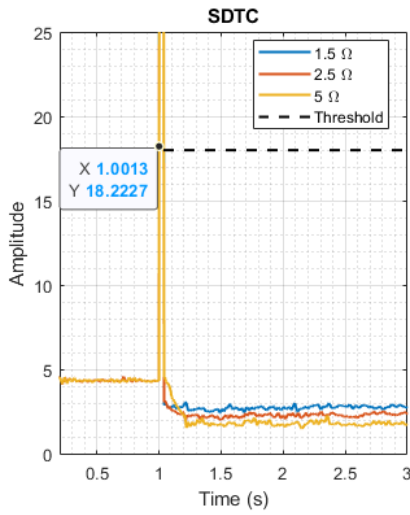
(b)

Fig. 11. Analysis of the proposed approach during PG fault scenario within the PV sources: a) 2D model, b) SDTC over time.

(a)

(b)

Fig. 12. Analysis of the proposed approach during PP fault scenario within the PV sources: a) 2D model, b) SDTC over time.

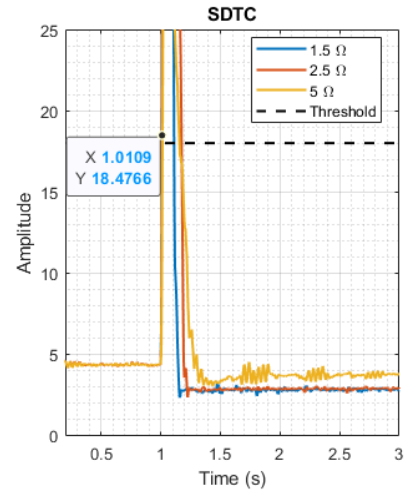### 3.2. Simulation results for implementing the proposed FL method

In this paper, the protection method benefits from a WOA-LSTM model to locate the faults occurring in the DCMG. As previously mentioned, we have used this technique to reduce the number of IEDs and prevent major blackouts in the microgrid. To evaluate this capability, several faults at various locations are applied on the line A. The faults are applied at different distances from 10% of the line and continue with a step of 5% up to 90%. Fault impedances of 1.5Ω, 2.5Ω, and 5Ω are also considered for a more complete investigation. Fig. 14 depicts the results of the proposed FL. Subsequently, Fig. 14-a shows the results obtained from the localization using the WOA-LSTM model, and Fig. 14-b shows the error value calculated using Eq. (18) for each case.

$$Error = |Refrencefaultlocation − Predictionfaultlocation| \quad (18)$$

It is evident that the LSTM model exhibits precise performance when faults occur on the main line A. However, given that the protection system utilizes only one IED, it is imperative to accurately identify FLs occurring in various areas of the microgrid and isolate only the faulty section. The evaluation results for different cases are presented in Table 3. It is evident that the

proposed protection algorithm demonstrates accurate performance under various conditions. By precisely detecting faulty areas, it effectively prevents further blackouts in the microgrid.

Finally, the optimized parameters of the LSTM model are presented in Table 4.

4. COMPARATIVE ANALYSIS: PROPOSED METHOD VERSUS ESTABLISHED FD TECHNIQUES IN DCMGS

4.1. Comparison during noisy signal conditions

The presence of noisy signal conditions poses significant challenges for FD methods in microgrids. This section conducts a comparison through computer simulations with the method presented in [37, 62, 63]. All simulations were conducted on the main DC bus with white Gaussian noise having a signal to noise ratio (SNR) of 40 dB. The performance of these three methods under noisy conditions is depicted in Fig. 15. In the proposed method described in [62], a fault is detected if the calculated signal value exceeds zero. However, as depicted in Fig. 15-a, when the fault has not been applied to the network, the calculated signal value exceeds zero. Consequently, this condition is erroneously identified as a fault in the microgrid. In the technique proposed in [63], which employs an intelligent method known as the Group Method of Data Handling (GMDH), a trip command is issued if
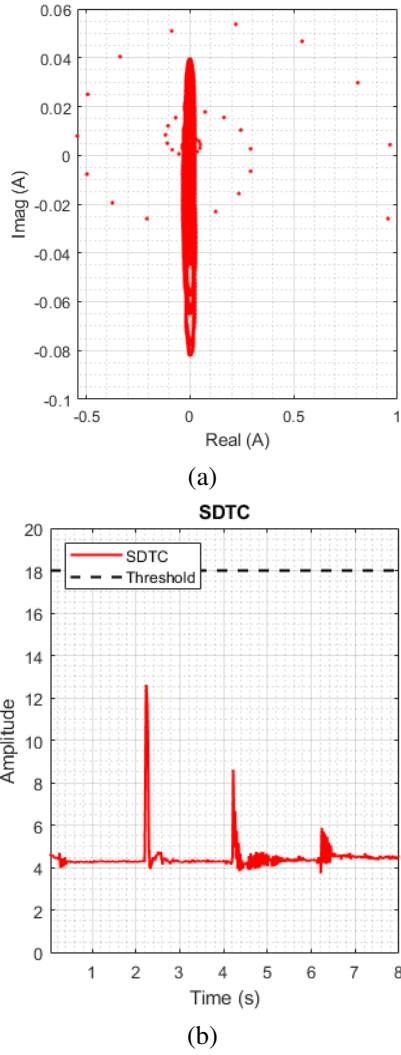
(a)

(b)

Fig. 13. Analysis of the proposed approach under transient states: a) 2D model, b) SDTC over time.
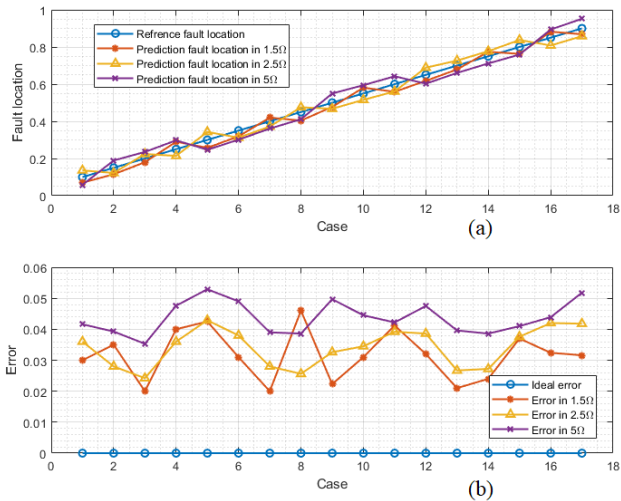

(a)

(b)

Fig. 14. Performance of the WOA-LSTM model for FL during different fault types: a) FL, b) FL error calculation by Eq. (18).

the signal error value estimated by the GMDH neural network

Table 2. Summary of evaluation results of the proposed method.

Fault location	Fault type	Fault impedance (Ω)	(ms)
DC bus	PG	1.5	1
		2.5	1
		5	1
	PP	1.5	1
		2.5	1
		5	1
Ev	PG	1.5	3
		2.5	3
		5	3
	PP	1.5	11
		2.5	11
		5	11
PV	PG	1.5	1
		2.5	1
		5	1
	PP	1.5	10
		2.5	10
		5	10
Transient states	-	-	No operation

Table 3. Summary of evaluation results of the proposed method.

Fault location	Fault type	Fault impedance (Ω)	Algorithm performance
Ev	PG	1.5	Correct
		2.5	Correct
		5	Correct
	PP	1.5	Correct
		2.5	Correct
		5	Correct
PV	PG	1.5	Correct
		2.5	Correct
		5	Correct
	PP	1.5	Correct
		2.5	Correct
		5	Correct
ESS	PG	1.5	Correct
		2.5	Correct
		5	Correct
	PP	1.5	Correct
		2.5	Correct
		5	Correct
Load	PG	1.5	Correct
		2.5	Correct
		5	Correct
	PP	1.5	Correct
		2.5	Correct
		5	Correct

exceeds the actual signal value. However, as depicted in Fig. 15-b, when noise is introduced into the signal, this method practically fails to distinguish between noise and an actual fault. In the technique proposed in [37], which employs a regression tree (RT), a trip command is issued if the signal error value estimated by the RT exceeds the zero value. However, as depicted in Fig. 15-c, when noise is introduced into the signal, this method practically fails to distinguish between noise and an actual fault.

Nevertheless, the method presented in this paper demonstrates accurate performance in detecting faults, even with varying impedances, under noisy conditions. It precisely distinguishes faults from noise in the microgrid. Fig. 16 illustrates the performance of the proposed method in noisy signal conditions.

4.2. Comparing the performance of various FD methods using only one IED

Since this paper utilizes only one IED for FD and FL across different areas of the microgrid, the authors have evaluated the performance of both the common single threshold high current method and the empirical mode decomposition (EMD) method introduced in [44] for protecting a DCMG using an IED. To conduct this study, PP and PG faults are applied to the EV installed in the sample microgrid at t=2 seconds. Subsequently, these two

Table 4. Optimized parameters of the proposed LSTM model.

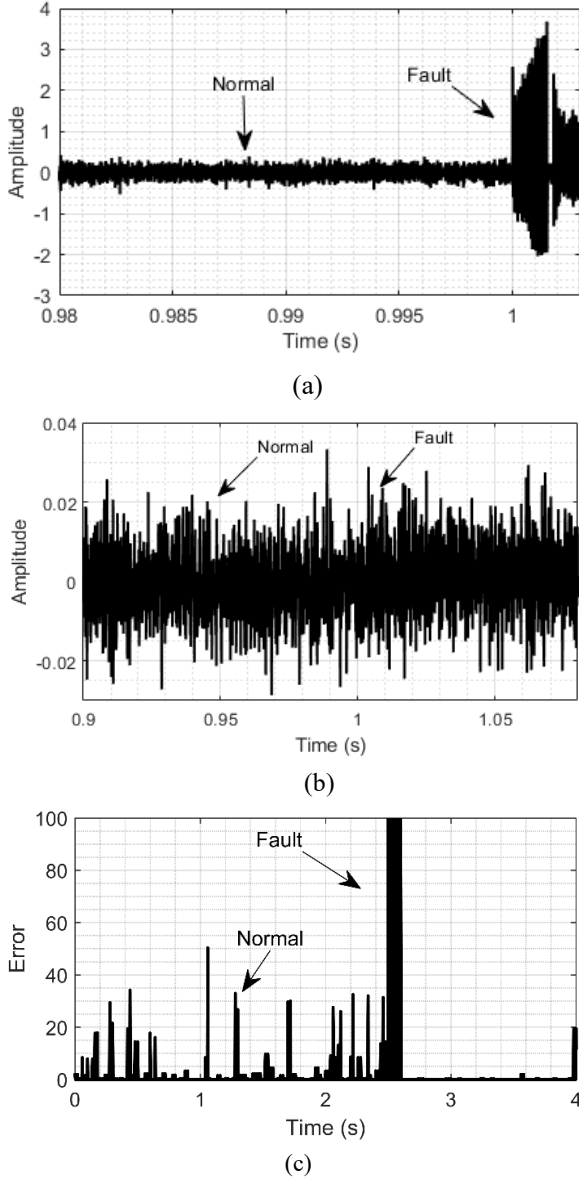| Parameter	Value
Number of LSTM layers	2
Number of neurons per layer	26, 18
Initial learning rate	0.0128
Learning rate drop factor	0.8000
Learning rate drop period	55
Min batch size	44
Dropout rate	0.200
Number of epochs	200

(a)

(b)

(c)

Fig. 15. Analysis of the three existing methods in noisy conditions, a) proposed method in [62], b) proposed method in [63], c) proposed method in [37].

types of faults are applied to the single threshold over current method and the EMD method. Fig. 17 illustrates the results of this investigation. The figure clearly demonstrates that both methods are unable to detect this type of fault. Consequently, there is a need to employ different IEDs for FD in various parts of the microgrid. In contrast, the method proposed in this paper, validated through numerous simulations, effectively detects various types of faults
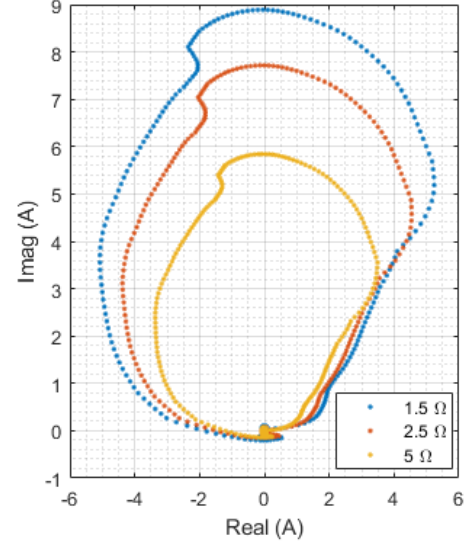
(a)
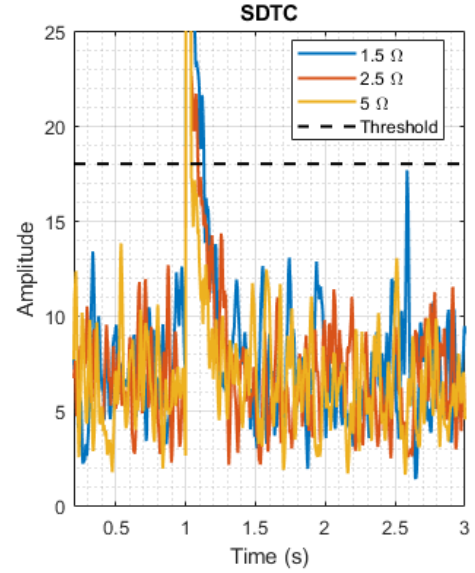
(b)

Fig. 16. Analysis of the proposed approach when the current signal is noisy: a) 2D model, b) SDTC over time.

occurring in different parts of the microgrid using a single IED.

4.3. Comparing the performance of fault location method

In order to locate the fault, the authors in [37] employ a feature extraction method based on the feature matrix. A comparison between the accuracy of the model presented in [37] and the model proposed in this paper is conducted using RMSE, MSE, and MAE parameters. The results of this comparison are depicted in Fig. 18. All results shown in this figure confirm the clear superiority of the method proposed in this paper in FL accuracy.

4.4. Comparative analysis of various features of the proposed method against other approaches

Table 5 shows the comparison between the proposed approach in this paper and existing microgrid protection methods. As evident from this table, besides considering the control system,

Table 5. Evaluation of the proposed approach against other existing techniques.

| Ref.	Publication year	Detection/Location	FD time		EV/PV	HESS	Hierarchical control system	Using a single IED
[37]	2024	Detection and location	>1 ms		✓	✓	✓	✓
[64]	2024	Detection and location	————-		✗	✗	✗	✗
[65]	2023	Detection	0.02 ms		✗	✗	✗	✓
[66]	2023	Detection and location	0.02 s		PV	✗	✗	✗
[67]	2023	Detection	1 ms		PV	✗	✗	✗
[68]	2022	Detection	250 ms		✗	✗	✓	✗
[69]	2021	Detection	3.95 ms		PV	✓	✗	✗
[70]	2020	Detection and location	1 ms		PV	✗	✗	✓
[63]	2019	Detection	8 ms		PV	✗	✗	✗
This paper	–	Detection and location	Fault in PV and EV 10–11 ms	Fault in DC bus 1 ms	✓	✓	✓	✓

(a)

(b)
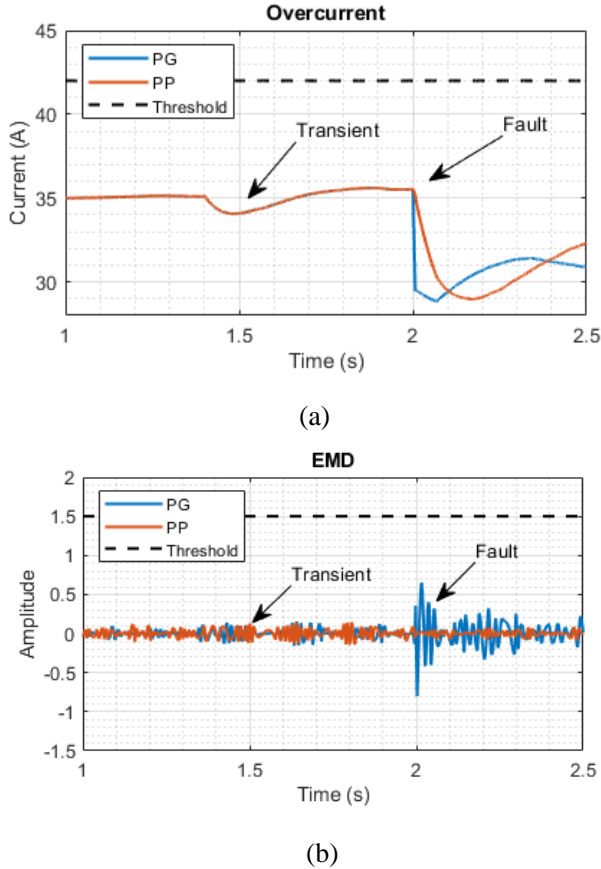
Fig. 17. Comparison of FD in EV with only one IED: a) single threshold overcurrent method b) EMD method presented in [44]

the proposed method also takes into account a fast HESS in the evaluations. Furthermore, the proposed protection method operates based on a single IED and does not require multiple IEDs and extensive communication links. According to the examination outcomes, the algorithm presented in this paper demonstrates a higher level of effectiveness compared to other existing methods. This method is fast and highly accurate in FD and FL.

5. DISCUSSION

In the preceding sections, the proposed method underwent a comprehensive evaluation utilizing MATLAB software and a sample DCMG. While the evaluation results and comparisons demonstrate significant progress, certain considerations remain. This section addresses issues such as the feasibility of implementation on practical hardware and performance on other existing topologies, such as DC ring microgrids. The hardware implementation of the proposed method can be discussed in two parts: one focusing on the FD method and the other on the intelligent FL method.
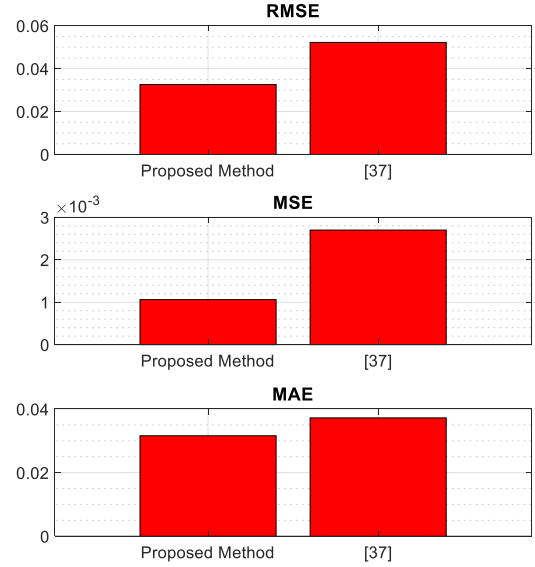

Fig. 18. Comparison of the accuracy of determining the location of the fault between the proposed method and the method presented in [37].

In the FD method, the use of conventional Fourier transform and the simplicity of the required calculations make it easily implementable on standard microprocessors. In contrast, the proposed WOA-LSTM method, with its associated complexities in implementation, requires more sophisticated hardware and microprocessors. The authors recommend utilizing the Zynq 7020 chip for this purpose. This chip combines the capabilities of FPGA with the processing power of ARM processors, making it highly suitable for applications that demand both digital signal processing (DSP) and microprocessor control. It is important to note that the WOA-LSTM model can be trained outside the microprocessor environment, and only the trained model needs to be deployed on the microprocessor for use. It is crucial to mention that implementing the proposed method on real hardware requires the use of the Python programming language and the TensorFlow Lite library. This library is specifically designed to execute machine learning models on microcontrollers and other devices with limited memory, typically only a few kilobytes. As for the application of the proposed method to various DCMG topologies, including the ring microgrid, it should be noted that the method is versatile and can operate in all types of DCMG configurations. Importantly, to apply the method to different microgrid topologies, one needs to recalculate the threshold value and retrain the WOA-LSTM model using new data.

In future work, the fault tolerance mechanisms discussed in [71] could be adapted and further explored to enhance the proposed method. Specifically, integrating passive and active fault-tolerant control strategies can provide a robust framework for addressing diverse fault scenarios in DC microgrids.

6. CONCLUSION

This paper presents an innovative method for FD and localization in a DCMG using the WOA-LSTM model. The approach begins by identifying faults in the microgrid through the comparison of the calculated SDTC value with a predefined threshold. Afterward, upon detecting the fault, the algorithm transfers the fault information to the pretrained WOA-LSTM model for fault localization. The proposed algorithm has been evaluated by employing a DCMG that includes EV, PV, and HESS. Various scenarios and a hierarchical control system have been fully implemented for the DCMG. These scenarios encompass a range of control system decisions contingent on various network conditions, such as alterations in the charging and discharging mode of the hybrid storage system, variations in the power consumption by loads, and the charging or discharging of EVs. The evaluation results of the proposed method demonstrate that this method is capable of rapidly detecting all fault types in different microgrids. Moreover, due to the presence of the FL algorithm, this method shortens the repair time in faulty areas within the microgrid. The proposed protection method uses one IED, eliminating the necessity for a communication system, to protect the DCMG. The deployment of the proposed method effectively identifies and pinpoints faults at various locations within the microgrid in as little as 1 millisecond and within PV and EV components in up to 11 milliseconds. This capability has been validated across a range of fault types and impedances. Additionally, the method has demonstrated reliable performance despite noisy conditions, maintaining accuracy with a signal to noise ratio of 40 dB. In contrast, several previous methods fail to perform reliably under such noisy conditions.

APPENDIX

Table 6. Sample DC microgrid parameters.

Parameter	Value
DC bus voltage	600 V
AC bus voltage	380 V
PV power	20 kW
Charging and discharging current of EV	15 A and 10 A
Battery	Life PO4, 360 V, 100 Ah
Flywheel	10 kW, 10000 r/min, 5000 r/min
AC loads	5 kW each load
DC load	5 kW
Cross section	240 mm^2
Cable resistance	0.125 Ω/km
Cable inductance	0.232 Ω/km
L1–L4 lines length	1 km

REFERENCES

[1] C. Patil, S. Thale, S. Muchande, and A. H. Kadam, "A novel protection scheme for dc microgrid with hierarchical control," in *2017 IEEE Int. Conf. Smart Energy Grid Eng.*, pp. 117–122, IEEE, 2017.

[2] R. Mohanty and A. K. Pradhan, "Protection of smart dc microgrid with ring configuration using parameter estimation approach," *IEEE Trans. Smart Grid*, vol. 9, no. 6, pp. 6328–6337, 2017.

[3] R. Dadi, K. Meenakshy, and S. Damodaran, "A review on secondary control methods in dc microgrid," *J. Oper. Autom. Power Eng.*, vol. 11, no. 2, pp. 105–112, 2023.

[4] E. Naderi, S. Seyedshenava, and H. Shayeghi, "High gain dc/dc converter implemented with mppt algorithm for dc microgrid system," *J. Oper. Autom. Power Eng.*, vol. 11, no. 3, pp. 213–222, 2023.

[5] S. Beheshtaein, R. M. Cuzner, M. Forouzesh, M. Savaghebi, and J. M. Guerrero, "Dc microgrid protection: A comprehensive review," *IEEE J. Emerg. Sel. Topics Power Electron.*, 2019.

[6] D. Marroqui, J. M. Blanes, A. Garrigos, and R. Gutierrez, "Self-powered 380 v dc sic solid-state circuit breaker and fault current limiter," *IEEE Trans. Power Electron.*, vol. 34, no. 10, pp. 9600–9608, 2019.

[7] L. Chen *et al.*, "Application and design of a resistive-type superconducting fault current limiter for efficient protection of a dc microgrid," *IEEE Trans. Appl. Supercond.*, vol. 29, no. 2, pp. 1–7, 2018.

[8] R. Eslami and S. A. Hosseini, "A comprehensive method for fault detection in ac/dc hybrid microgrid," *Electr. Power Compon. Syst.*, vol. 50, no. 1-2, pp. 38–51, 2022.

[9] R. Eslami and S. Hosseini, "Presenting new triple methods for fault detection, location, and its identification in dc microgrid," *Iran. J. Sci. Technol. Trans.Electr. Eng.*, vol. 44, pp. 849–860, 2020.

[10] D. Salomonsson, L. Soder, and A. Sannino, "Protection of low-voltage dc microgrids," *IEEE Trans. Power Del.*, vol. 24, no. 3, pp. 1045–1053, 2009.

[11] A. Shabani and K. Mazlumi, "Evaluation of a communication-assisted overcurrent protection scheme for photovoltaic-based dc microgrid," *IEEE Trans. Smart Grid*, vol. 11, no. 1, pp. 429–439, 2019.

[12] S. K. Maurya, A. K. Soni, A. Mohapatra, and A. Sharma, "Optimal single settings based relay coordination in dc microgrids for line faults," *Int. J. Electr. Power Energy Syst.*, vol. 156, p. 109708, 2024.

[13] S.-A. Amamra, H. Ahmed, and R. A. El-Sehiemy, "Firefly algorithm optimized robust protection scheme for dc microgrid," *Electr. Power Compon. Syst.*, vol. 45, no. 10, pp. 1141–1151, 2017.

[14] S. Augustine, M. J. Reno, S. M. Brahma, and O. Lavrova, "Fault current control and protection in a standalone dc microgrid using adaptive droop and current derivative," *IEEE J. Emerg. Sel. Topics Power Electron.*, vol. 9, no. 3, pp. 2529–2539, 2020.

[15] E. Christopher, M. Sumner, D. W. Thomas, X. Wang, and F. de Wildt, "Fault location in a zonal dc marine power system using active impedance estimation," *IEEE Trans. Ind. Appl.*, vol. 49, no. 2, pp. 860–865, 2013.

[16] K. Jia, Q. Zhao, T. Feng, and T. Bi, "Distance protection scheme for dc distribution systems based on the high-frequency characteristics of faults," *IEEE Trans. Power Deliv.*, vol. 35, no. 1, pp. 234–243, 2019.

[17] R. Montoya, B. P. Poudel, A. Bidram, and M. J. Reno, "Dc microgrid fault detection using multiresolution analysis of traveling waves," *Int. J. Electr. Power Energy Syst.*, vol. 135, p. 107590, 2022.

[18] K. Saleh, A. Hooshyar, and E. F. El-Saadany, "Fault detection and location in medium-voltage dc microgrids using travelling-wave reflections," *IET Renew. Power Gener.*, vol. 14, no. 4, pp. 571–579, 2020.

[19] I. Almutairy and M. Alluhaidan, "Fault diagnosis based approach to protecting dc microgrid using machine learning technique," *Procedia Comput. Sci.*, vol. 114, pp. 449–456, 2017.

[20] P. Pan and R. K. Mandal, "Fault detection and classification in dc microgrid clusters," *Eng. Res. Express*, vol. 5, no. 2, p. 025010, 2023.

[21] K. Anjaiah, P. K. Dash, and M. Sahani, "A new protection scheme for pv-wind based dc-ring microgrid by using modified multifractal detrended fluctuation analysis," *Prot. Control Mod. Power Syst.*, vol. 7, no. 1, p. 8, 2022.

[22] S. Dhar and P. K. Dash, "Differential current-based fault protection with adaptive threshold for multiple pv-based dc microgrid," *IET Renew. Power Gener.*, vol. 11, no. 6, pp. 778–790, 2017.

[23] M. Li, Y. Luo, K. Jia, T. Bi, and Q. Yang, "Frequency-based current differential protection for vsc-mvdc distribution lines," *Int. J. Electr. Power Energy Syst.*, vol. 117, p. 105626, 2020.

[24] W. Zhang, H. Zhang, and N. Zhi, "A novel protection strategy for dc microgrid considering communication failure," *Energy Rep.*, vol. 9, pp. 2035–2044, 2023.

[25] R. Rahmani, S. H. H. Sadeghi, H. Askarian-Abyaneh, and M. J. Emadi, "An entropy-based scheme for protection of dc microgrids," *Electr. Power Syst. Res.*, vol. 228, p. 110010, 2024.

[26] Z. Moravej, A. Ebrahimi, and M. Barati, "A new differential protection scheme based on synchro-squeezing transform applied to ac micro-grid," *Electr. Power Syst. Res.*, vol. 231, p. 110336, 2024.

[27] K. Ding *et al.*, "Feature extraction and fault diagnosis of photovoltaic array based on current–voltage conversion," *Appl. Energy*, vol. 353, p. 122135, 2024.

[28] A. Amiri, H. Samet, and T. Ghanbari, "Recurrence plots based method for detecting series arc faults in photovoltaic systems," *IEEE Trans. Ind. Electron.*, vol. 69, no. 6, pp. 6308–6315, 2021.

[29] M. Xu, L. Xiao, and H. Wang, "A prony-based method of locating short-circuit fault in dc distribution system," 2013.

[30] D. Jayamaha, N. Lidula, and A. Rajapakse, "Protection and grounding methods in dc microgrids: Comprehensive review and analysis," *Renew. Sust. Energ. Rev.*, vol. 120, p. 109631, 2020.

[31] R. Mohanty, U. S. M. Balaji, and A. K. Pradhan, "An accurate noniterative fault-location technique for low-voltage dc microgrid," *IEEE Trans. Power Deliv.*, vol. 31, no. 2, pp. 475–481, 2015.

[32] A. Meghwani, S. C. Srivastava, and S. Chakrabarti, "Local measurement-based technique for estimating fault location in multi-source dc microgrids," *IET Gener. Transm. Distrib.*, vol. 12, no. 13, pp. 3305–3313, 2018.

[33] Y. Yang, C. Huang, D. Zhou, and Y. Li, "Fault detection and location in multi-terminal dc microgrid based on local measurement," *Electr. Power Syst. Res.*, vol. 194, p. 107047, 2021.

[34] M. A. Aftab, S. S. Hussain, I. Ali, and T. S. Ustun, "Dynamic protection of power systems with high penetration of renewables: A review of the traveling wave based fault location techniques," *Int. J. Electr. Power Energy Syst.*, vol. 114, p. 105410, 2020.

[35] S. Dhar, R. K. Patnaik, and P. Dash, "Fault detection and location of photovoltaic based dc microgrid using differential protection strategy," *IEEE Trans. Smart Grid*, vol. 9, no. 5, pp. 4303–4312, 2017.

[36] Q. Yang, J. Li, S. Le Blond, and C. Wang, "Artificial neural network based fault detection and fault location in the dc microgrid," *Energy Procedia*, vol. 103, pp. 129–134, 2016.

[37] S. Salehimehr, S. M. Miraftabzadeh, and M. Brenna, "A novel machine learning-based approach for fault detection and location in low-voltage dc microgrids," *Sustainability*, vol. 16, no. 7, p. 2821, 2024.

[38] C. Li, P. Rakhra, P. J. Norman, G. M. Burt, and P. Clarkson, "Multi-sample differential protection scheme in dc microgrids," *IEEE J. Emerg. Sel. Top. Power Electron.*, vol. 9, no. 3, pp. 2560–2573, 2020.

[39] S. Z. Jamali *et al.*, "A high-speed fault detection, identification, and isolation method for a last mile radial lvdc distribution network," *Energies*, vol. 11, no. 11, p. 2901, 2018.

[40] L. Zhang, N. Tai, W. Huang, J. Liu, and Y. Wang, "A review on protection of dc microgrids," *J. Mod. Power Syst. Clean Energy*, vol. 6, no. 6, pp. 1113–1127, 2018.

[41] S. Wang, T. Bi, and K. Jia, "Wavelet entropy based fault detection approach for mmc-hvdc lines," in *2015 IEEE Power Energy Society General Meeting*, pp. 1–5, IEEE, 2015.

[42] M. Shaban, M. A. Mosa, A. Ali, and K. Abdel-Latif, "Effect of power sharing control techniques of hybrid energy storage system during fault conditions in dc microgrid," *J. Energy Storage*, vol. 72, p. 108249, 2023.

[43] L. Shen, Q. Cheng, Y. Cheng, L. Wei, and Y. Wang, "Hierarchical control of dc micro-grid for photovoltaic ev charging station based on flywheel and battery energy storage system," *Electr. Power Syst. Res.*, vol. 179, p. 106079, 2020.

[44] B. Taheri and A. Shahhoseini, "Direct current (dc) microgrid control in the presence of electrical vehicle/photovoltaic (ev/pv) systems and hybrid energy storage systems: A case study of grounding and protection issue," *IET Gener. Transm. Distrib.*, 2023.

[45] M. T. Sadiq, X. Yu, Z. Yuan, and M. Z. Aziz, "Motor imagery bci classification based on novel two-dimensional modelling in empirical wavelet transform," *Electron. Lett.*, vol. 56, no. 25, pp. 1367–1369, 2020.

[46] S. Hochreiter, Y. Bengio, P. Frasconi, and J. Schmidhuber, "Gradient flow in recurrent nets: the difficulty of learning long-term dependencies," in *A Field Guide to Dynamical Recurrent Neural Networks*, IEEE Press, 2001.

[47] S. Hochreiter and J. Schmidhuber, "Long short-term memory," *Neural Comput.*, vol. 9, no. 8, pp. 1735–1780, 1997.

[48] K. Greff, R. K. Srivastava, J. Koutník, B. R. Steunebrink, and J. Schmidhuber, "Lstm: A search space odyssey," *IEEE Trans. Neural Netw. Learn. Syst.*, vol. 28, no. 10, pp. 2222–2232, 2016.

[49] C. Zhang *et al.*, "Multi-imbalance: An open-source software for multi-class imbalance learning," *Knowl.-Based Syst.*, vol. 174, pp. 137–143, 2019.

[50] F. Huang, X. Zhang, Z. Li, Z. Zhao, and Y. He, "From content to links: Social image embedding with deep multimodal model," *Knowl.-Based Syst.*, vol. 160, pp. 251–264, 2018.

[51] Y. Wu, H. Mao, and Z. Yi, "Audio classification using attention-augmented convolutional neural network," *Knowl.-Based Syst.*, vol. 161, pp. 90–100, 2018.

[52] C. Zhang, C. Liu, X. Zhang, and G. Almpanidis, "An up-to-date comparison of state-of-the-art classification algorithms," *Expert Syst. Appl.*, vol. 82, pp. 128–150, 2017.

[53] S. Salehimehr, B. Taheri, and M. Sedighizadeh, "Short-term load forecasting in smart grids using artificial intelligence methods: A survey," *J. Eng.*, vol. 2022, no. 12, pp. 1133–1142, 2022.

[54] B.-S. Kwon, R.-J. Park, and K.-B. Song, "Short-term load forecasting based on deep neural networks using lstm layer," *J. Electr. Eng. Technol.*, vol. 15, pp. 1501–1509, 2020.

[55] P. Wang, J. Zhao, Y. Gao, M. A. Sotelo, and Z. Li, "Lane work-schedule of toll station based on queuing theory and pso-lstm model," *IEEE Access*, vol. 8, pp. 84434–84443, 2020.

[56] X. Ren, S. Liu, X. Yu, and X. Dong, "A method for state-of-charge estimation of lithium-ion batteries based on pso-lstm," *Energy*, vol. 234, p. 121236, 2021.

[57] B. Shao, M. Li, Y. Zhao, and G. Bian, "Nickel price forecast based on the lstm neural network optimized by the improved pso algorithm," *Math. Probl. Eng.*, vol. 2019, 2019.

[58] N. Xu, X. Wang, X. Meng, and H. Chang, "Gas concentration prediction based on iwoa-lstm-ceemdan residual correction model," *Sensors*, vol. 22, no. 12, p. 4412, 2022.

[59] S. Mirjalili and A. Lewis, "The whale optimization algorithm," *Adv. Eng. Softw.*, vol. 95, pp. 51–67, 2016.

[60] L. Shao, Q. Guo, C. Li, J. Li, and H. Yan, "Short-term load forecasting based on eemd-woa-lstm combination model," *Appl. Bionics Biomech.*, vol. 2022, 2022.

[61] N. J. Marand, H. S. Daliri, and H. Askarian-Abyaneh, "Removal of dc offset components by using two auxiliary signals," in *2023 IEEE PES GTD Int. Conf. Expo.*, pp. 226–230, IEEE, 2023.

[62] M. Dashtdar, O. Rubanenko, D. Danylchenko, S. M. S. Hosseinimoghadam, N. K. Sharma, and M. Baiai, "Protection of dc microgrids based on differential protection method by fuzzy systems," in *2021 IEEE 2nd KhPI Week Adv. Technol.*, pp. 22–27, IEEE, 2021.

[63] B. Taheri, S. A. Hosseini, S. Salehimehr, and F. Razavi,

"A novel approach for detection high impedance fault in dc microgrid," in *2019 Int. Power Syst. Conf.*, pp. 287–292, IEEE, 2019.

[64] G. Li *et al.*, "Analysis and fault location of single-pole ground fault in lvdc ungrounded system," in *4th Int. Conf. Mech., Electron., Electr. Autom. Control*, vol. 13163, pp. 953–959, SPIE, 2024.

[65] P. Pan and R. K. Mandal, "Intelligent short-circuit protection with solid-state circuit breakers for low-voltage dc microgrids," *IETE J. Res.*, pp. 1–17, 2023.

[66] C. Zhang, H. Wang, Z. Wang, and Y. Li, "Active detection fault diagnosis and fault location technology for lvdc distribution networks," *Int. J. Electr. Power Energy Syst.*, vol. 148, p. 108921, 2023.

[67] S. Sanati, M. Azzouz, and A. Awad, "An adaptive overcurrent protection for solar-based dc microgrids using iec 61850,"

arXiv preprint arXiv:2307.01940, 2023.

[68] M. Mola, A. Afshar, N. Meskin, and M. Karrari, "Distributed fast fault detection in dc microgrids," *IEEE Syst. J.*, vol. 16, no. 1, pp. 440–451, 2020.

[69] N. K. Sharma, S. R. Samantaray, and C. N. Bhende, "Vmd-enabled current-based fast fault detection scheme for dc microgrid," *IEEE Syst. J.*, vol. 16, no. 1, pp. 933–944, 2021.

[70] Y. R. O, S. Chatterjee, A. K. Chakraborty, and A. R. Bhowmik, "Fault detection and location estimation for lvdc microgrid using self-parametric measurements," *Int. Trans. Electr. Energy Syst.*, vol. 30, no. 9, p. e12499, 2020.

[71] L. Ortiz, J. W. González, L. B. Gutierrez, and O. Llanes-Santiago, "A review on control and fault-tolerant control systems of ac/dc microgrids," *Heliyon*, vol. 6, no. 8, 2020.